Humanized substitutions of *Vmat1* in mice alter amygdala-dependent behaviors associated with the evolution of anxiety

Daiki X. Sato[1, #†], Yukiko U. Inoue[2†], Yuki Morimoto[2], Takayoshi Inoue[2], Nahoko Kuga[3], Takuya Sasaki[3, 4], Yuji Ikegaya[3, 5, 6], Kensaku Nomoto[7], Takefumi Kikusui[8], Satoko Hattori[9], Giovanni Sala[9], Hideo Hagihara[9], Tsuyoshi Miyakawa[9] and Masakado Kawata[1]*

[1]Graduate School of Life Sciences, Tohoku University, Sendai, Miyagi 980-8578, Japan
[2]Department of Biochemistry and Cellular Biology, National Institute of Neuroscience, National Center of Neurology and Psychiatry, Kodaira, Tokyo 187-8502, Japan
[3]Graduate School of Pharmaceutical Sciences, The University of Tokyo, 7-3-1 Hongo, Bunkyo-Ku, Tokyo 113-0033, Japan
[4]Precursory Research for Embryonic Science and Technology (PRESTO), Japan Science and Technology Agency (JST), 4-1-8 Honcho, Kawaguchi, Saitama 332-0012, Japan
[5]Center for Information and Neural Networks, National Institute of Information and Communications Technology, 1-4 Yamadaoka, Suita City, Osaka, 565-0871, Japan
[6]Institute for AI and Beyond, The University of Tokyo, Tokyo 113-0033, Japan
[7]Department of Physiology, Dokkyo Medical University, Mibu, Tochigi, 321-0293, Japan
[8]Department of Animal Science and Biotechnology, Azabu University, Kanagawa, Japan
[9]Division of Systems Medical Science, Institute for Comprehensive Medical Science, Fujita Health University, Toyoake, Aichi 470-1192, Japan
[#]Present address: Graduate School of Science, Chiba University, Chiba, 263-8522, Japan

[†]equally contributed
*corresponding author: kawata@tohoku.ac.jp, TEL +81-22-795-6688

Keywords
Vmat1, anxiety, amygdala, human evolution, CRISPR/Cas9

Abstract

The human vesicular monoamine transporter 1 (*VMAT1*) harbors unique substitutions (Asn136Thr/Ile) that affect monoamine uptake into synaptic vesicles. These substitutions are absent in all known mammals, suggesting their contributions to distinct aspects of human behavior modulated by monoaminergic transmission, such as emotion and cognition. To directly test the impact of these human-specific mutations, we introduced the humanized residues into mouse *Vmat1* via CRISPR/Cas9-mediated genome editing and examined changes at the behavioral, neurophysiological and molecular levels. Behavioral tests revealed reduced anxiety-related traits of *Vmat1*^{Ile} mice, consistent with human studies, and electrophysiological recordings showed altered oscillatory activity in the amygdala under anxiogenic conditions. Transcriptome analyses further identified amygdala-specific changes in the expression of genes involved in neurodevelopment and emotional regulation, which may corroborate the observed phenotypes. This knock-in mouse model hence provides compelling evidence that the mutations affecting monoaminergic signaling and amygdala circuits have contributed to the evolution of human socio-emotional behaviors.

50 **Introduction**

51 Recent years have seen a surge in the study revealing distinct human brain
52 characteristics at the molecular, cellular, and circuit levels in both cortex and subcortical
53 structures (1–4). Differences in brain monoaminergic signaling are likely to be key
54 factors conferring human attributes, as various monoaminergic pathways are involved in
55 emotional regulation, memory consolidation, cognitive flexibility, and complex social
56 behaviors (5–7). Comparative studies have indeed demonstrated the distinct
57 monoaminergic mechanisms in the human brain (2, 8). Moreover, diversification of
58 monoaminergic mechanisms has been linked to the evolution of social behavior in non-
59 human primates (9, 10). Thus, genetic differentiation of monoaminergic genes may
60 underlie our unique emotional and social characteristics, such as empathy and altruism
61 (2).

62 In line with these studies, we recently reported that the vesicular monoamine
63 transporter 1 (*VMAT1*; also known as *SLC18A1*) gene has been under positive selection
64 in the human lineage as evidenced by two amino acid substitutions (Glu130Gly and
65 Asn136Thr) not shared by other primates (11). The VMATs transport monoamine
66 neurotransmitters into synaptic vesicles, thereby regulating the kinetics of synaptic
67 transmission. There are two isoforms of VMAT, VMAT1 and 2, with the VMAT2
68 being highly expressed in the brain and widely studied (12, 13). In contrast, VMAT1
69 was previously thought to be expressed solely in the peripheral nervous system and
70 chromaffin cells, and its functional importance in the CNS has only recently been
71 implicated (14). Our previous study showed that a new mutation at the 136th amino

72 acid (136Ile) of *VMAT1* has emerged relatively recently in the course of human
73 evolution, and that the human-specific polymorphism Thr136Ile has likely been
74 maintained by balancing selection within non-African populations (11). Fluorometric
75 assays additionally demonstrated that these human-specific residues enhance
76 monoamine neurotransmitter uptake, suggesting the tendency of lower monoamine
77 uptake in early hominids (15). The 136Thr, the dominant variant across populations, is
78 known to be marginally associated with psychiatric diseases, such as bipolar disorder,
79 depression and anxiety, as well as with the neuroticism, a personality trait conferring
80 greater risk of psychiatric disease (16–18). Thus, higher levels of depression and/or
81 anxiety-like behaviors with 136Thr may have been favored in our ancestors, while more
82 recent selection may have led to the emergence of 136Ile after the migration out of
83 Africa and into harsher environments.

84 Although the evolution of *VMAT1* and its basic functions in the mammalian
85 CNS have been clarified, their contributions to unique human attributes are still unclear.
86 Here we examine the molecular, neurological, and behavioral changes in mice caused
87 by human-specific *VMAT1* mutations. We show that humanized *Vmat1* (*Vmat1*^{Ile})
88 induces amygdala-specific changes in gene expression and neuronal activity, reduces
89 anxiety-like behaviors under anxiogenic conditions and even enhances preference for
90 social novelty. These findings suggest that altered monoaminergic signaling in the
91 amygdala has contributed to the evolution of human emotional and social behaviors,
92 and the present work provides a new experimental strategy for evolutionary studies of
93 human emotions.

Results

Conservation of the 136th residue of VMAT1 across non-human vertebrates

To investigate the evolutionary significance of the 136th residue in human VMAT1 (hVMAT1), we first examined the conservation of this residue in a wide range of taxa in vertebrates. Multiple sequence alignments of VMAT1 among 236 vertebrate species revealed the unique evolution of this residue in the human lineage (Fig. 1a). Notably, we confirmed that all species but bicolor damselfish retain asparagine (Asn) at the 136th amino acid, while *Homo sapiens* is the only vertebrate species that carries the unique Thr136Ile (rs1390938) polymorphism.

Predicted effects of humanized residues on mouse VMAT1 structure and function

In silico predictions of wild type mouse VMAT1 (mVMAT1) protein structure revealed that like the hVMAT1 residue 136, the corresponding residue in mVMAT1 (133Asn) was located between the first luminal loop and the second transmembrane domain (Fig. 1b), suggesting a similar function. Given the evolutionary conservation across vertebrates and the difference in chemical properties between amino acids, the humanized mutations to mVMAT1, especially 133Asn to 133Ile, were predicted to have a significant impact on protein function (Table 1). Furthermore, the Asn133Ile mutation was also predicted to stabilize the protein structure as evidenced by greater folding free energy ($\Delta\Delta G$: 1.106 kcal/mol; Table 1) and to increase the flexibility of the loop domain (Fig. 1b), which possibly increases the efficiency of monoamine uptake.

116

117 **Generation of *Vmat1*-humanized mouse models by CRISPR/Cas9 genome editing**

118 In order to replace the 133Asn of mouse Vmat1 with Thr or Ile, we employed the
119 CRISPR/Cas9-mediated genome editing strategy (Fig. 2a). We selected a guide RNA
120 targeting the 133rd Asn codon in *Vmat1* exon 4 by using the web-based CRISPR design
121 tool to minimize off-target cleavage risk (Supplementary Table S1 and 2, see Methods
122 for details). By electroporating CRISPR components (*Vmat1* exon 4 crRNA, tracrRNA,
123 and Cas9 nuclease) along with the ssDNA donor containing the desired substitutions
124 into C57BL/6J fertilized eggs (Fig 2a, Supplementary Fig S1a), we successfully
125 generated 133Thr founder No.1 and 133Ile founder No.10 (Supplementary Fig. S1b, c
126 and d). After confirming the absence of off-target cleavages (Supplementary Fig. S2),
127 we crossed 133Thr founder No.1 and 133Ile founder No.10 with wild type (WT)
128 C57BL/6J mice to obtain heterozygous F1 generations, which were again verified to
129 possess the designed substitutions by Sanger sequencing. The homozygous mice were
130 further crossed after the F5 generations to obtain three humanized genotypes, Thr/Thr,
131 Thr/Ile, and Ile/Ile, in addition to WT, for behavioral, neurophysiological, and
132 transcriptomic analyses (Supplementary Fig. S3, see Methods).

133

134 **The human Ile substitution in mVMAT1 reduced behavioral anxiety**

135 We accordingly conducted comprehensive behavioral tests among the 20 sets of mice
136 including one of each genotype (*Vmat1*^{WT}, *Vmat1*$^{Thr/Thr}$, *Vmat1*$^{Thr/Ile}$, and *Vmat1*$^{Ile/Ile}$)
137 from the 1st batch at 9–55 weeks (see Supplementary Table S3 for detailed information

138 on age and the number of individuals used in each test). Detailed results were shown in
139 Fig. S4–19. Tests of social interaction (SI) between stranger mice of the same genotype
140 in a novel environment (one-chamber SI test) and of preference for a novel stranger
141 over a previously exposed stranger (now familiar) in Crawley's 3-chamber social
142 interaction (CSI) test revealed marginal differences in behavioral phenotypes between
143 mice with and without *Vmat1*^{Ile} (P = 0.062 for interactive effects of genotype (Ile) and
144 place, generalized additive model (GAM) with quasi-Poisson distribution; Fig. 3a,
145 Supplementary Fig. S9 and 10). In the CSI, *Vmat1*$^{Thr/Thr}$ mice significantly preferred
146 familiar to stranger mice ($P = 3.26\times10^{-4}$), while no such tendency was observed in
147 *Vmat1*^{Ile} mice (P = 0.759 for *Vmat1*$^{Thr/Ile}$ mice and (P = 0.195 for *Vmat1*$^{Ile/Ile}$ mice; Fig.
148 3a). Moreover, we found consistently lower levels of anxiety among *Vmat1*^{Ile} mice
149 across tests, including relatively greater preference for the (anxiogenic) light box during
150 the two-chamber light/dark transition (LD) test and for the center of an open field (OF)
151 (Supplementary Fig. S5 and 6).
152 To confirm a pervasive effect on specific behavioral domains by humanized
153 VMAT1, we constructed composite behavioral phenotype scores by summating
154 standardized scores on related tests (LD, OF, elevated plus maze (EP), and SI tests) and
155 compared the results among genotypes. We further conducted Structural Equation
156 Modeling (SEM) to investigate the effects of genotype on these composite scores. This
157 analysis revealed a significant effect of 133Ile on anxiety scores (R^2 = 0.15, $P = 8.7\times10^{-}$
158 ^{3}) but only marginal effects on locomotor activity (R^2 = 0.062, P = 0.053; Fig. 3b).

159 Anxiety levels were generally lower in *Vmat1*^{Ile} mice (P = 0.016, one-way ANOVA;
160 Fig 3c).
161 In addition to standard tests of anxiety, exploratory tendency, and locomotor
162 activity, we also performed a novel delayed reward task to evaluate the differences in
163 impulsivity between *Vmat1*$^{Thr/Thr}$ and *Vmat1*$^{Ile/Ile}$ mice (n = 10 for both genotypes, see
164 Methods for detailed experimental procedure; Supplementary Fig. S19a–c). Throughout
165 the test, there was no statistically significant difference in food preference between
166 genotypes (P = 0.50 for the first term, GAM with quasi-Poisson distribution;
167 Supplementary Fig. S19d). However, *Vmat1*$^{Ile/Ile}$ showed a lower preference for the
168 higher-calorie but delayed food reward than *Vmat1*$^{Thr/Thr}$ mice every test day from 5 to 9
169 except for day 6 compared to the basal level after habituation (day 4) (Supplementary
170 Fig. S19d).
171
172 **Differential regulation of dopaminergic and neurodevelopmental genes in the**
173 **amygdala by *Vmat1* genotype**
174 We then conducted RNA-Seq analysis to investigate the effects of the four *Vmat1*
175 genotypes on gene expression patterns in three brain regions likely associated with the
176 behavioral phenotypes (prefrontal cortex, amygdala, and striatum) (n = 4 mice for each
177 genotype; see Supplementary Table S4 for detailed information on samples and reads).
178 Principal component analysis revealed distinct expression patterns among brain areas,
179 but no obvious differences between genotypes and ages (4 vs. 10 months)
180 (Supplementary Fig. S20).

181 We thus screened for differentially expressed genes (DEGs) by pair-wise
182 comparisons between genotypes, which yielded a total of 80 DEGs exclusively in the
183 amygdala (Fig. 4a). A large proportion of these genes (56 out of 80) were differentially
184 expressed between *Vmat1*^{WT} and *Vmat1*$^{Ile/Ile}$ mice (Fig. 4a). The expression levels of
185 DEGs for each sample were shown in Supplementary Fig. S21. We then utilized the
186 correlations between individual composite anxiety scores and expression levels of the
187 detected amygdalar DEGs among a subset of 8 mice (n = 2 for each genotype).
188 Particularly strong correlations were found for nine genes, *Baz1a*, *Camk2n1*, *Ccdc114*,
189 *Cldn1*, *Fsbp*, *Gdnf*, *Gm42608*, *Gsg1l*, and *KI* ($P < 0.1$; Fig. 4b, Supplementary Fig.
190 S22). The DEGs were further examined for gene ontology (GO) enrichment, which
191 revealed significant overrepresentation of genes involved in "behavior", "fear
192 response", "response to amphetamine", "cardiac muscle tissue development", or
193 "cAMP catabolic process" (Table 2) between WT and Ile/Ile mice, while no GO terms
194 were enriched in DEGs for other genotype comparisons (as there were few such genes).
195 Moreover, gene expression patterns in the Ile mice amygdala were significantly
196 positively correlated with those of striata of transgenic mouse models of Huntington
197 disease ($P < 1.0 \times 10^{-28}$; Supplementary Table S5, Fig. S23).
198 To further characterize the biological pathways affected by *Vmat1* genotype,
199 we performed weighted gene correlation network analysis (WGCNA; Fig. 4c). A co-
200 expressing gene module (M1; Fig. 4c) stood out as it was significantly overrepresented
201 with DEGs detected in the WT vs. Ile/Ile comparison (odds ratio = 3.79, $P = 2.88\times10^{-8}$
202 by Fisher's exact test) and was negatively correlated with composite anxiety score.

203 These genes include many involved in adrenergic (*Adra2b*), dopaminergic (*Adcy5*,
204 *Adora2a*, *Drd1*, *Drd2*, *Gnal*, *Gng7*, *Gpr6*, *Gpr88*, *Pde1b*, *Pde1c*, *Pde7b*, *Pde10a*, *Pdyn*,
205 *Penk*, *Ppp1r1b*, *Rasgrp2*, *Rgs9* and *Tac1*), glutamatergic (*Grm4*), and serotonergic
206 (*Htr1b*, *Htr1d*, *Htr1f*, and *Htr4*) signaling pathways. Sub-network analysis further
207 detected another functional gene cluster involved in neural development within the co-
208 expressing module (cluster 2 in Fig. 4d). Strikingly, three genes, *Foxp1*, *Foxp2*, or *Six3*,
209 all of which are important regulators of neural growth, were located in hubs connecting
210 genes involved in postsynaptic signaling (cluster 1) as mentioned above and neural
211 development (cluster 2; e.g., *Dlx6*, *Ebf1*, *Isl1*, and Wnt2).
212

213 **The humanized mVMAT1 disrupted anxiety-associated theta band activity in the**
214 **basolateral amygdala**

215 Aforementioned behavioral and transcriptomic results suggest that the *Vmat1* genotype
216 influences anxiety-related neuronal activity patterns. Inspired by a previous report that
217 theta (4–12 Hz) oscillations in the medial prefrontal cortex (mPFC) and basolateral
218 amygdala (BLA) are specifically enhanced under anxiogenic environments such as the
219 open arms of an elevated plus maze (EP) and the center area of an OF (19, 20), we next
220 performed simultaneous local field potential (LFP) recordings from the dorsomedial
221 prefrontal cortex (dmPFC) and BLA in freely moving mice during elevated plus maze
222 (EP) exploration (Fig. 5a; n = 11 dmPFC and 9 BLA electrodes from 5 *Vmat1*^{WT}, n = 6
223 and 6 electrodes from 4 *Vmat1*$^{Thr/Thr}$ and n = 10 and 7 electrodes from 4 *Vmat1*$^{Ile/Ile}$
224 mice). The histological confirmation of electrode positions and raw LFP signals were

225 shown in Fig. 5b and c, respectively. Power spectral analysis of WT mice revealed
226 lower 4–7 Hz power in both dmPFC and BLA during exploration of the EP open arms
227 compared to close arms, suggesting a relationship with anxiety-like behavior (Fig. 5d).
228 Further, the Granger causality test revealed the directionality of 4–7 Hz oscillations
229 from the mPFC to BLA (Fig. 5e; n = 20 electrode pairs from 5 *Vmat1*^{WT} mice),
230 consistent with anatomical evidence that the dmPFC preferentially projects to the BLA
231 (21, 22) and that mPFC theta oscillations drive BLA neuronal activity (20). Based on
232 these observations, we compared 4–7 Hz power in dmPFC and BLA among genotypes.
233 Both WT and *Vmat1*$^{Thr/Thr}$ mice exhibited significantly lower LFP 4–7 Hz signal power
234 in dmPFC and BLA under the anxiogenic condition of open arm exploration compared
235 to closed arm exploration, while *Vmat1*$^{Ile/Ile}$ mice showed no such consistent activity
236 pattern in the BLA (Fig. 5f), suggesting that anxiety-related neuronal mechanisms in the
237 dmPFC–BLA circuit are disrupted by the *Vmat1*$^{Ile/Ile}$ genotype.
238

239 **Discussion**

240 While the potential importance of *VMAT1* in neuroendocrine signaling has been
241 suggested, few studies have focused on this gene until recently, largely due to its low
242 expression in the central nervous system (12, 23, 24). A series of studies, however, have
243 demonstrated the psychopathological effects of this gene and suggests its importance in
244 emotional regulation. The Thr136Ile polymorphism (rs1390938) is allegedly associated
245 with bipolar disorder (16), autism spectrum disorder (25), cognitive function related to
246 schizophrenia (26), anxiety, depressiveness, neuroticism, or maladaptive impulsivity

247 (18). Our previous study uncovered from an evolutionary perspective that this variant is
248 a human-specific polymorphism (as shown in Fig. 1a) and under positive selection in
249 the human lineage (11). Two substitutions (i.e., Glu130Gly and Asn136Thr) occurred in
250 the human lineage after the divergence from the common ancestor of chimpanzees and
251 humans, and these substitutions combined have been shown to decrease the monoamine
252 uptake of VMAT1 (15). On the other hand, the new "hyper-function" allele (i.e. 136Ile;
253 Lohoff et al. 2014), which increases the monoamine uptake of VMAT1 and is
254 associated with fewer psychopathological symptoms by contrast, emerged just before
255 the Out-of-Africa event of modern humans and is currently 20–61% in frequency in
256 non-African populations (11). We also found that the Thr136Ile polymorphism has been
257 under balancing selection in non-African populations (11). Given such evolutionary
258 significance and psychopathological effects of the Thr136Ile polymorphism in *VMAT1*,
259 this variant could play a very important role in exploring the evolutionary origins of
260 human psychological traits and their diversity.
261
262 **Phenotypic changes in mice caused by the humanized *Vmat1***
263 Our comprehensive behavioral tests show the protective effects of the $Vmat1^{Ile}$ allele
264 against anxiety-like behavior (Fig. 3b and c), which is well consistent with the human
265 phenotype (18). Compared to $Vmat1^{Ile}$ ($Vmat1^{Thr/Ile}$ and $Vmat1^{Ile/Ile}$) mice, both wild-
266 type and $Vmat1^{Thr/Thr}$ mice showed similar behavioral phenotypes and have higher levels
267 of anxiety in both solitary (LD, EP, and OF) and social (SI and CSI) environment. This
268 is expected from the molecular evidence that 136Asn and 136Thr are comparable in the

269 level of monoamine uptake, which is lower than that of 136Ile (15). It is noteworthy that
270 the genotypic effect was not observed for fear response of mice (Supplementary Fig.
271 S16). Given the potential difference in neurological mechanism behind fear and anxiety
272 (27, 28), Vmat1 may specifically regulate anxiety-related circuits of the brain as
273 discussed later. The results of delayed reward task may suggest that the *Vmat1*$^{Ile/Ile}$ mice
274 are more impulsive, at least initially, under this condition but contradicts an
275 epidemiological study reporting an association of 136Thr with maladaptive impulsivity
276 (18). Kim et al. (2018) reported that the deletion of the D2 dopamine receptor (D2R)
277 increased impulsive behavior in mice, whereas restoration of D2R in the amygdala
278 alone normalized impulsive behavior (29). This is compatible with our results, as
279 dopaminergic genes including *Drd2* were downregulated in *Vmat1*$^{Ile/Ile}$ mice
280 (Supplementary Fig. S24). The possible difference in association of *VMAT1* genotype
281 with impulsivity between humans and mice may stem from functional connectivity
282 changes in related neural circuits and warrants further investigation. Overall, these
283 observations suggest that the 136Ile substitution may contribute to uniquely human
284 behavioral traits that have propelled both our technological progress and adaptation to
285 almost all ecosystems, namely high exploratory tendency and relatively lower anxiety
286 under threatening or novel conditions. Indeed, 136Ile allele frequency increases along
287 the migration route of modern humans (11), suggesting that the exploratory tendency
288 and/or boldness conferred by this mutation was advantageous for survival. In this
289 regard, *Vmat1*^{Ile} is analogous to the D4R polymorphism associated with novelty-seeking
290 behavior (30).

291 Differentially expressed genes were significantly enriched in those
292 downregulated in *Vmat1*$^{Ile/Ile}$ and involved in behavioral control and/or fear response as
293 well Huntington disease (HD). It is possible that the Ile mice recapitulate some
294 dimensions of HD pathology, given that dopamine (DA) signaling likely plays a
295 significant role in HD, and the only current FDA-approved drug for HD is a VMAT2
296 inhibitor, tetrabenazine (31). WGCNA detected a co-expressing module (M1; Fig. 4c)
297 in which the DEGs were significantly overrepresented and revealed that many genes
298 involved in monoaminergic signaling pathways were co-expressed with the detected
299 DEGs (Fig. 4d). Lohoff et al. reported that *Vmat1* KO affected DA signaling in
300 particular, with upregulation of D2R and downregulation of tyrosine hydroxylase (TH)
301 observed in both the frontal cortex and striatum (32). Given the association between
302 *Vmat1* KO and decreased DA in the frontal cortex, we speculated that *Vmat1*$^{Ile/Ile}$ mice
303 would also exhibit downregulation of D2R and upregulation of TH compared to WT
304 mice. Indeed, D2R (along with many other dopaminergic pathway genes) was
305 downregulated in *Vmat1*$^{Ile/Ile}$ mice compared to WT mice. However, there were no
306 significant differences in TH expression among genotypes (Supplementary Fig. S24),
307 suggesting that the *Vmat1* Ile allele alters dopaminergic transmission but not DA
308 synthesis. The sub-network analysis detected another functional gene cluster involved in
309 neural development within the co-expressing module (cluster 2 in Fig. 4d), such as
310 *Foxp1*, *Foxp2*, *Six3*, *Dlx6*, *Ebf1*, *Isl1*, and *Wnt2*. Foxp1 (forkhead box protein P1) is a
311 transcription factor that regulates the development of various tissues including the brain.
312 Foxp1 heterodimerizes with Foxp2, and a human-specific Foxp2 substitution is

313 associated with language impairment (33, 34). Foxp2 also regulates D2R expression
314 (35) and extracellular DA levels (34), potentially involved in the neural development
315 (36), while the cluster 2 genes *Dlx6*, *Ebf1*, *Isl1*, and *Six*3 are all implicated in the
316 development of striatal neurons that express DA receptors (37–39). The DEG Wnt2
317 (also known as Irp) has been found to increase dopaminergic neurons by inducing the
318 proliferation of progenitor cells in the developing midbrain (40). The differential
319 expression of these genes may also be related to the regulatory role of VMAT1 in
320 hippocampal neurogenesis (41), which emerging evidence suggests is associated with
321 anxiety-like behavior (42, 43). Taken together, the differential regulation of DA
322 signaling by *Vmat1* genotypes may have widespread effects on neural development and
323 plasticity.

324 The electrophysiological analysis revealed abnormal neuronal activity in the
325 amygdala of *Vmat1*$^{Ile/Ile}$ mice under fearful conditions (i.e., open arms in EP test; Fig.
326 5f). This was not seen in the medial prefrontal cortex, and thus suggests that amygdala-
327 specific neuronal disturbance underlies the reduced anxiety-like behavior associated
328 with this genotype. This is consistent with a functional imaging study showing that
329 136Ile was associated with increased reactivity and decreased habituation of amygdala
330 toward threat-related stimuli in humans (14). Additional studies are required to reveal
331 the precise association between these LFP changes and amygdalar output in *Vmat1*^{Ile}
332 mice. In light of our behavioral results, we suggest that *Vmat1*^{Ile} may promote the
333 activity of neurons that dampen anxiety, such those projecting from the BLA to the
334 central amygdala (44, 45).

335

336 **Amygdala-specific transcriptomic and neuronal changes associated with anxiety**

337 **imply intra- and inter-species differences in emotion and social behavior**

338 One of the major findings of this study is that *Vmat1* genotype affected transcriptomic

339 regulation and neuronal activity primarily in the amygdala. Given that amygdalar DA

340 signaling is a powerful modulator of fear and anxiety (46), the alterations in gene

341 expression and oscillatory neuronal activity likely contribute to the observed reduction

342 in anxiety-like behaviors among *Vmat1*^{Ile} mice compared to WT mice. The abnormal

343 neuronal activity pattern detected in the amygdala but not PFC of *Vmat1*^{Ile} mice may

344 stem from a difference in VMAT1 expression levels across the brain. Previous studies

345 verified that *VMAT1* mRNA and protein expression levels are relatively high in the

346 amygdala compared to other brain regions in both rats and humans (16, 47). Our

347 transcriptome analysis also revealed higher expression of *Vmat1* in the amygdala than in

348 the striatum (P = 0.0097, Dunnett's test; Supplementary Fig. S25). In contrast, *Vmat2*

349 expression was comparable across regions (Supplementary Fig. S25), indicating

350 distinctive regional regulation between subtypes as shown in a previous study (41).

351 However, the detailed transcriptomic effects of Vmat1 on various types of neurons

352 within the amygdala and possible contributions of peripheral monoamine signaling to

353 them are still unclear, and thus need to be investigated with greater spatial resolution in

354 future studies.

355 Neuronal circuits within the amygdala store associations between

356 environmental cues and adverse stimuli as changes in synaptic strength, and these

357 modified circuits drive the expression of emotion-related behaviors and physiological
358 responses. Thus, the amygdala is a critical regulator of emotional and social behaviors
359 (48), and in fact amygdalar dysfunction is implicated in a number of neuropsychiatric
360 disorders (49–51). Although it is an evolutionarily primitive brain region with relatively
361 well conserved gross structure and general function across species (45), recent studies
362 have provided evidence for more subtle structural and/or functional differences within
363 and among species potentially linked to differential regulation of monoaminergic
364 signaling via VMAT1. The size of the amygdala has been shown to correlate with
365 creativity (52) , mental state inference (53), and the size and complexity of social
366 networks in humans (54) and non-human primates (55). The DA response in the medial
367 amygdala network is associated with mother–infant bonding (56). Collectively, these
368 findings strongly suggest a substantial contribution of the amygdala to evolution of the
369 human social brain by acting as a hub among brain networks associated with emotion,
370 cognition, and communication (57).
371

372 **A single substitution in humanized mouse models highlight molecular and**
373 **neurological evolution underlying human emotional traits**

374 Genetic deletion (KO) and overexpression have become predominant strategies for
375 examining the neurological, behavioral, and pathogenic functions of specific genes.
376 However, gene deletion and overexpression may alter the expression levels of many
377 additional genes, and thus the observed phenotype may be distinct from that induced by
378 target-specific pharmacological manipulations. The present study employed an

379 alternative "knock-in" strategy of a non-synonymous *Vmat1* mutation and succeeded in
380 capturing moderate differences in transcriptomic, neuronal, and behavioral phenotypes.
381 Noticeably, the variant evaluated is a human-specific substitution (i.e., Thr136Ile of
382 *VMAT1*) under selection that is not possessed by other mammals (Fig. 1a). This knock-
383 in model thus provides a unique opportunity to examine the molecular and neurological
384 mechanisms that distinguish human behavior from that of other primates. Such
385 extensive functional analysis of a single mutation has been limited to a few genes such
386 as *FOXP2* (34, 58) and never for effects on emotional traits (59). Therefore, the present
387 study is the first to suggest a new experimental strategy for studies on the evolution of
388 human brain mechanisms underlying emotion and related behavioral traits.
389 Lastly, it needs to be noted that recent genome-wide association studies
390 (GWAS) on psychiatric disorders such as depression (60) and schizophrenia (61), and
391 on specific personality traits (62) have not detected VMAT1 as a top hit despite alleged
392 associations with these phenotypes under study (18, 63). This may indicate that
393 VMAT1 has a weaker influence on phenotype than other significant loci, or that this
394 gene must interact with other loci (epistasis) and/or environmental factors (G × E
395 interaction) for measurable effects on phenotype. Such dependence on other genes or
396 external factors could obscure phenotypic associations of VMAT1 evaluated by
397 conventional approaches of GWAS. In fact, we found that a single amino acid
398 substitution (Asn133Ile) altered the expression of 56 genes within the amygdala, any or
399 all of which may contribute to the observed changes in behavioral phenotype. The
400 effects of various environmental factors (which were largely controlled in this

401 experiment through group housing and shared dams) and DEGs on these behavioral and

402 neurological phenotypes would warrant further study.

403 **Methods**

404 Fully detailed and referenced methods are available in Supplementary Methods.

405

406 **Phylogenetic analysis and *in silico* prediction of mVMAT1 structure with**

407 **humanized residues**

408 A phylogenetic tree was constructed from 263 orthologous sequences of vertebrate

409 *SLC18A1* (*VMAT1*), including an archaic hominin sequence that was constructed by

410 replacing 136Ile in the human reference sequence with 136Thr. Homology modeling of

411 the mouse VMAT1 (mVMAT1) protein structure was performed using the SWISS-

412 MODEL (64) web server (http://swissmodel.expasy.org) with the visualization by using

413 PyMOL 2.4.1 (DeLanoScientific, San Carlos, CA). Provean v1.1.3 (65) and SIFT (66)

414 were used to estimate the intolerance for individual amino acid mutations introduced in

415 mVMAT1 based on the evolutionary conservation and the chemical properties of the

416 exchanged residues. DynaMut (67) was also used to evaluate the effects of humanized

417 mutations on the stability and flexibility of VMAT1 protein structure.

418

419 **Generation of *Vmat1*-humanized mouse models by CRISPR/Cas9 genome editing**

420 See Supplementary Methods for the detailed design and preparation of guide RNA and

421 single-strand DNA (ssDNA) donors targeting mouse *Vmat1*. In addition to the intended

422 humanization, the synonymous substitutions depicted in Fig. 2a were introduced near

423 the 133rd site to prevent unwanted re-editing and enable PCR genotyping. The guide

424 RNAs, Cas9 proteins, and the donor ssDNAs were electroporated into mouse zygotes

425 following the standard protocol (68) to obtain founder knock-in mice (Supplementary
426 Fig S1a). The 133Thr and 133Ile knock-in founders were screened by PCR-RFLP assay
427 (Supplementary Fig. S1c), followed by Sanger sequencing to confirm the correct
428 substitution (Supplementary Fig. S1d). To exclude the possible side effects from off-
429 target cleavages, we sequenced 12 more potential off-target candidate loci predicted by
430 CRISPOR (69) (http://crispor.org) (Supplementary Table S2, Supplementary Fig. S2).
431 After confirming the absence of off-target cleavages, 133Thr founder No.1 and
432 133Ile founder No.10 were crossed with WT C57BL/6J mice to obtain heterozygous F1
433 generations, which were again verified to possess the designed substitutions by Sanger
434 sequencing. For behavioral tests, F5 or F6 homozygous mice were crossed to obtain
435 Thr/Thr, Thr/Ile, and Ile/Ile genotypes. In addition, C57BL/6J WT males and females
436 carrying the Asn/Asn genotype were crossed to supply control mice. To eliminate
437 differences in rearing environment, newborn males of the 4 genotypes (Asn/Asn,
438 Thr/Thr, Thr/Ile, and Ile/Ile) were grouped in sets and nursed by the same mothers.
439
440 **Animal care and experimental conditions for behavioral tests**
441 Animals were housed in groups of four individuals of each genotype under a 12 h
442 light/dark cycle (7:00 AM to 7:00 PM) with ad libitum access to food and water. Adult
443 male mice were used in all tests to eliminate the behavioral effects of the estrus cycle.
444 The composition of cohorts and ages of the mice for every experiment are summarized
445 in Supplementary Table S3. All behavioral tests were conducted in a soundproof room,
446 and as much effort as possible was spent on controlling the effects of confounding

447 factors such as light intensity, temperature, and humidity for the tested group of cage
448 mates. Furthermore, to minimize the impact of one test on subsequent tests in individual
449 mice, behavioral assessments were conducted in the following order after general health
450 and neurological screens: light/dark transition (LD), open field (OF), elevated plus maze
451 (EP), hot plate, social interaction in a novel environment (SI), rotarod, Crawley's 3-
452 chamber social interaction test (CSI), startle response/prepulse inhibition, Porsolt forced
453 swim, T-maze, Barnes maze, tail suspension, fear conditioning, and home cage social
454 interaction tests. See Supplementary Methods for detailed descriptions of behavioral
455 tests.

456 All animal care protocols and experiments were performed according to
457 guidelines approved by the Animal Care and Use Committee of the National Institute of
458 Neuroscience, National Center of Neurology and Psychiatry (approval numbers:
459 2017005, 2020007), the Animal Experiment Committee of Fujita Health University
460 (approval number: APU19063), and the Experimental Animal Ethics Committees of
461 Graduate School of Medicine, and the University of Tokyo (approval number: P29-14).
462

463 **Statistical analyses and Structural Equation Modeling (SEM)**

464 In order to capture overall behavioral patterns among genotypes, we analyzed two major
465 domains of mouse behavior, activity and anxiety, by standardizing, normalizing, and
466 combining sets of related behavioral scores. Total distances traveled in LD, OF, EP, SI,
467 and CSI were used as indices for activity, while time in the light compartment of the LD
468 shuttle box, duration in the central area of the OF, time spent in open arms of the EP,

469 and total duration of active contacts in the SI were used as indices of anxiety. To
470 confirm the effects of *Vmat1* genotype on the behavioral composites and to enhance
471 statistical power and improve reliability, we used Structural Equation Modeling (SEM)
472 (70). The SEM model included a measurement model and a regression model. The
473 measurement model consisted of two latent factors grouping tests of locomotor activity
474 and anxiety-like behavior. The regression model evaluated the effect of genotype on the
475 two latent factors. Goodness of model fit was evaluated by normed Comparative Fit
476 Index (CFI), Root Mean Square Error of Approximation (RMSEA), and the
477 Standardized Root Mean Square Residual (SRMR) and significance of paths was tested
478 by *t*-test. Normalization of behavioral scores and SEM were performed using the
479 *bestNormalize* and *lavaan* packages in R, respectively.
480
481 ***In vivo* electrophysiological recordings and histological analysis**
482 Five male WT C57BL/6J mice (16–20 weeks old, SLC Shizuoka, Japan) with
483 preoperative weights of 20–30 g as well as four male *Vmat1*$^{Ile/Ile}$ mice (16–20 weeks
484 old) and four male *Vmat1*$^{Thr/Thr}$ mice (20–24 weeks old) obtained from the 2nd batch
485 were implanted with intracranial electrodes for *in vivo* electrophysiological recordings.
486 The animals were housed under a 12 h/12 h light/dark schedule with lights on at 7:00
487 AM prior to surgery. For local field potential (LFP) recordings, an array of 3 immobile
488 tetrodes was stereotaxically implanted above the dmPFC (2.00 mm anterior and 0.50
489 mm lateral to bregma) at a depth of 1.40 mm and an array of 4 tetrodes was implanted
490 in the amygdala (0.80 mm posterior and 3.00 mm lateral to bregma) at a depth of 4.40

491 mm using guide cannulae. Following surgery, each animal was housed in a separate
492 transparent Plexiglas cage with free access to water and food for at least 7 days before
493 recordings.
494 The mouse was connected to the recording equipment via a digitally
495 programmable amplifier (Cereplex M, Blackrock Microsystems, Salt Lake City, UT)
496 placed close to the animal's head. Electrical signals during elevated plus maze (see
497 methods for detail) were sampled at 2 kHz and low-pass filtered at 500 Hz with
498 Cereplex Direct data acquisition system. The animal's moment-to-moment position was
499 tracked at 15 Hz using a video camera attached to the ceiling for 10 min. After a
500 recording session, the mouse was overdosed with isoflurane, perfused intracardially
501 with 4% paraformaldehyde (PFA) in phosphate-buffered saline (PBS, pH 7.4), and
502 decapitated. The dissected brain was fixed overnight in 4% PFA/PBS and then
503 cryoprotected by successive overnight incubations in 20% sucrose and 30% sucrose in
504 PBS. Frozen coronal sections (100 μm) were cut using a microtome, mounted, and
505 processed for cresyl violet staining. The positions of all electrodes were confirmed by
506 identifying the corresponding electrode tracks in histological tissue sections.
507
508 **RNA-sequencing and transcriptome analysis**
509 We obtained RNA-sequencing (RNA-seq) data from 3 tissues in the brain, prefrontal
510 cortex, amygdala, and striatum of four mice per genotype, with DNBSEQ platform at
511 the Beijing Genomics Institute (BGI, Hong Kong, China). The raw reads were quality
512 checked, trimmed, and filtered using fastp 0.20.0 (71), yielding 20–21 million filtered

513 reads per sample (Supplementary Table S4). STAR v2.7.5c (72) was then used for
514 mapping the reads to the reference mouse genome (GRCm38.p6). We assigned reads to
515 the Ensembl100 annotation and generated fragment counts by featureCounts (73), and
516 the fragment counts were used to perform differential expression analysis with iDEP
517 v0.91 workflow (74). After normalizing all counts according to effective library size,
518 we retained genes with > 1 count per million (CPM) in half of the samples (24
519 samples). A total of 13,608 genes were then assessed in downstream analyses. Principal
520 component analysis (PCA) was first performed to reveal the overall expression pattern
521 of each sample. While most samples demonstrated distinct expression patterns, one
522 supposed amygdala sample (derived from a 4-month-old *Vmat1*$^{Thr/Thr}$ mouse) exhibited
523 an expression pattern similar to the other striatal samples (Supplementary Fig. S20).
524 Given the inconsistency in the expression pattern, we excluded this sample and
525 conducted the normalization step again for the remaining 47 samples.
526 We conducted pair-wise between-genotype comparisons of the same brain
527 regions to identify differentially expressed genes (DEGs), which were defined by
528 |log2(fold change)| > 1 and false discovery rate (FDR; corrected by the Benjamini and
529 Hochberg method) < 0.05. The DEGs were further characterized by enrichment analysis
530 for gene ontology (GO) terms in the iDEP pipeline. An Illumina BaseSpace application
531 (http://basespace.illumina.com/apps) was used to investigate the correlation in
532 expression levels of DEGs among currently and previously collected datasets. To
533 identify specific biological pathways affected by *Vmat1* genotypes, we conducted
534 weighted gene correlation network analysis (WGCNA) (75) of 15 samples from the

535 amygdala. The 1000 genes with most variable expression levels (largest coefficients of
536 variation) among samples were retained, and the correlations among gene expression
537 levels across samples were then calculated to detect co-expressing modules. We also
538 calculated the correlations between the expression levels of a given gene in the
539 amygdala and the behavioral composite (locomotor activity and anxiety), based on the
540 data collected from 8 individuals (two for each genotype). Genes belonging to modules
541 of interest were further included in protein-protein interaction networks constructed
542 using STRING, and functional gene clusters were detected by the MCODE module of
543 Cytoscape 3.8.2 (76).

544 **Acknowledgments**

545 Some of the computations for transcriptomic analyses were performed on the NIG
546 supercomputer at ROIS National Institute of Genetics. We thank Dr. Liu Jinsha and Ms.
547 Eriko Koike for technical assistance with mouse embryo manipulations and care of
548 newborns, Ms. Chikako Ozeki and Tamaki Murakami for their assistance with
549 behavioral experiments, and Drs. Masayuki Koganezawa and Noriko Osumi for their
550 valuable comments on the manuscript. This work was supported by the Japan Society
551 for the Promotion of Science (Grants-in-Aid for Scientific Research 17H05934,
552 19H04892, and 16H06276 (AdAMS) to MK, 20J12055 to DXS, 17H05939 and
553 19H04897 to TS, 17H05967 and 19H04922 to YUI, and 16H06276 to TM) and
554 Intramural Research Grants for Neurological and Psychiatric Disorder of NCNP (27-7,
555 30-9, and 3-9 to TI). This work was also supported by MEXT Promotion of Distinctive
556 Joint Research Center Program (Grant Number JPMXP0618217663).

557

558 **Author contributions**

559 DXS and MK conceived and DXS, YUI, SH, TK, and TS designed the study. DXS,
560 YUI, TI, TM, TS, and MK acquired funding. YUI and YM conducted genome-editing
561 experiments with mice. DXS, SH, KN, and TK designed and DXS and SH performed
562 behavioral tests. DXS analyzed behavioral test results with the help of SH and GS. NK
563 and TS performed electrophysiological and histological experiments. TS dissected all
564 the brain samples for RNA-Seq, for which DXS and HH performed data analysis. DXS,

YUI, TI, SH, TS, and MK wrote the manuscript with contributions and revisions from all authors. All authors have read and approved the final manuscript.

Competing interest statement

The authors declare no competing interests.

570 **References**

571 1. A. M. M. Sousa, K. A. Meyer, G. Santpere, F. O. Gulden, N. Sestan, Evolution
572 of the human nervous system function, structure, and development. *Cell* **170**,
573 226–247 (2017).
574 2. M. A. Raghanti, *et al.*, A neurochemical hypothesis for the origin of hominids.
575 *Proc. Natl. Acad. Sci. U. S. A.* **115**, E1108–E1116 (2018).
576 3. Y. Zhu, *et al.*, Spatiotemporal transcriptomic divergence across human and
577 macaque brain development. *Science* **362**, eaat8077 (2018).
578 4. R. Pryluk, Y. Kfir, H. Gelbard-Sagiv, I. Fried, R. Paz, A tradeoff in the neural
579 code across regions and species. *Cell* **176**, 1–13 (2019).
580 5. R. Cools, A. C. Roberts, T. W. Robbins, Serotoninergic regulation of emotional
581 and behavioural control processes. *Trends Cogn. Sci.* **12**, 31–40 (2008).
582 6. D. Shohamy, R. A. Adcock, Dopamine and adaptive memory. *Trends Cogn. Sci.*
583 **14**, 464–472 (2010).
584 7. R. P. Ebstein, S. Israel, S. H. Chew, S. Zhong, A. Knafo, Genetics of human
585 social behavior. *Neuron* **65**, 831–844 (2010).
586 8. A. M. M. Sousa, Y. Zhu, M. A. Raghanti, R. R. Kitchen, M. Onorati, Molecular
587 and cellular reorganization of neural circuits in the human lineage. *Science* **358**,
588 1027–1032 (2017).
589 9. C. M. Bergey, J. E. Phillips-Conroy, T. R. Disotell, C. J. Jolly, Dopamine
590 pathway is highly diverged in primate species that differ markedly in social
591 behavior. *Proc. Natl. Acad. Sci. U. S. A.* **113**, 6178–6181 (2016).

592 10. N. Staes, *et al.*, Serotonin receptor 1A variation is associated with anxiety and
593 agonistic behavior in chimpanzees. *Mol. Biol. Evol.* **36**, 1418–1429 (2019).
594 11. D. X. Sato, M. Kawata, Positive and balancing selection on SLC18A1 gene
595 associated with psychiatric disorders and human-unique personality traits. *Evol.*
596 *Lett.* **2**, 499–510 (2018).
597 12. J. D. Erickson, M. K.-H. Schäfer, T. I. Bonner, L. E. Eiden, E. Weihe, Distinct
598 pharmacological properties and distribution in neurons and endocrine cells of two
599 isoforms of the human vesicular monoamine transporter. *Proc. Natl. Acad. Sci.*
600 *U. S. A.* **93**, 5166–5171 (1996).
601 13. K. M. Lohr, *et al.*, Increased vesicular monoamine transporter enhances
602 dopamine release and opposes Parkinson disease-related neurodegeneration in
603 vivo. *Proc. Natl. Acad. Sci. U. S. A.* **111**, 9977–82 (2014).
604 14. F. W. Lohoff, *et al.*, Functional genetic variants in the vesicular monoamine
605 transporter 1 modulate emotion processing. *Mol. Psychiatry* **19**, 129–139 (2014).
606 15. D. X. Sato, Y. Ishii, T. Nagai, K. Ohashi, M. Kawata, Human-specific mutations
607 in VMAT1 confer functional changes and multi-directional evolution in the
608 regulation of monoamine circuits. *BMC Evol. Biol.* **19**, 220 (2019).
609 16. F. W. Lohoff, *et al.*, Variations in the vesicular monoamine transporter 1 gene
610 (VMAT1/SLC18A1) are associated with bipolar I disorder.
611 *Neuropsychopharmacology* **31**, 2739–2747 (2006).
612 17. F. W. Lohoff, *et al.*, Association between variation in the vesicular monoamine
613 transporter 1 gene on chromosome 8p and anxiety-related personality traits.

614 *Neurosci. Lett.* **434**, 41–45 (2008).

615 18. M. Vaht, E. Kiive, T. Veidebaum, J. Harro, A functional vesicular monoamine
616 transporter 1 (VMAT1) gene variant is associated with affect and the prevalence
617 of anxiety, affective, and alcohol use disorders in a longitudinal population-
618 representative birth cohort study. *Int. J. Neuropsychopharmacol.* **19**, 1–9 (2016).

619 19. A. Adhikari, M. A. Topiwala, J. A. Gordon, Synchronized Activity between the
620 Ventral Hippocampus and the Medial Prefrontal Cortex during Anxiety. *Neuron*
621 **65**, 257–269 (2010).

622 20. E. Likhtik, J. M. Stujenske, M. A. Topiwala, A. Z. Harris, J. A. Gordon,
623 Prefrontal entrainment of amygdala activity signals safety in learned fear and
624 innate anxiety. *Nat. Neurosci.* **17**, 106–113 (2014).

625 21. O. Bukalo, *et al.*, Prefrontal inputs to the amygdala instruct fear extinction
626 memory formation. *Sci. Adv.* **1**, 1–9 (2015).

627 22. P. L. A. Gabbott, T. A. Warner, P. R. L. Jays, P. Salway, S. J. Busby, Prefrontal
628 cortex in the rat: Projections to subcortical autonomic, motor, and limbic centers.
629 *J. Comp. Neurol.* **492**, 145–177 (2005).

630 23. D. Peter, *et al.*, Differential expression of two vesicular monoamine transporters.
631 *J. Neurosci.* **15**, 6179–6188 (1995).

632 24. B. Schütz, M. K. H. Schäfer, L. E. Eiden, E. Weihe, Vesicular amine transporter
633 expression and isoform selection in developing brain, peripheral nervous system
634 and gut. *Dev. Brain Res.* **106**, 181–204 (1998).

635 25. R. Noroozi, *et al.*, Association study of the vesicular monoamine transporter 1

636 (VMAT1) gene with autism in an Iranian population. *Gene* **625**, 10–14 (2017).

637 26. A. C. Need, *et al.*, Pharmacogenetics of antipsychotic response in the CATIE
638 trial: a candidate gene analysis. *Eur. J. Hum. Genet.* **17**, 946–957 (2009).

639 27. M. Davis, D. L. Walker, L. Miles, C. Grillon, Phasic vs sustained fear in rats and
640 humans: Role of the extended amygdala in fear vs anxiety.
641 *Neuropsychopharmacology* **35**, 105–135 (2010).

642 28. P. Tovote, J. P. Fadok, A. Lüthi, Neuronal circuits for fear and anxiety. *Nat. Rev.*
643 *Neurosci.* **16**, 317–331 (2015).

644 29. B. Kim, *et al.*, Dopamine D2 receptor-mediated circuit from the central amygdala
645 to the bed nucleus of the stria terminalis regulates impulsive behavior. *Proc.*
646 *Natl. Acad. Sci. U. S. A.* **115**, E10730–E10739 (2018).

647 30. L. J. Matthews, P. M. Butler, Novelty-seeking DRD4 polymorphisms are
648 associated with human migration distance Out-of-Africa after controlling for
649 neutral population gene structure. **145**, 382–389 (2011).

650 31. J. Y. Chen, E. A. Wang, C. Cepeda, M. S. Levine, Dopamine imbalance in
651 Huntington's disease: A mechanism for the lack of behavioral flexibility. *Front.*
652 *Neurosci.* **7**, 1–14 (2013).

653 32. F. W. Lohoff, G. V. Carr, B. Brookshire, T. N. Ferraro, I. Lucki, Deletion of the
654 vesicular monoamine transporter 1 (vmat1/slc18a1) gene affects dopamine
655 signaling. *Brain Res.* **1712**, 151–157 (2019).

656 33. W. Enard, *et al.*, Molecular evolution of FOXP2, a gene involved in speech and
657 language. *Nature* **418**, 869–872 (2002).

658 34. W. Enard, *et al.*, A humanized version of Foxp2 affects cortico-basal ganglia
659 circuits in mice. *Cell* **137**, 961–971 (2009).
660 35. E. Spiteri, *et al.*, Identification of the transcriptional targets of FOXP2, a gene
661 linked to speech and language, in developing human brain. *Am. J. Hum. Genet.*
662 **81**, 1144–1157 (2007).
663 36. S. C. Vernes, *et al.*, Foxp2 regulates gene networks implicated in neurite
664 outgrowth in the developing brain. *PLoS Genet.* **7**, e1002145 (2011).
665 37. B. Wang, T. Lufkin, J. L. R. Rubenstein, Dlx6 regulates molecular properties of
666 the striatum and central nucleus of the amygdala. *J. Comp. Neurol.* **519**, 2320–
667 2334 (2011).
668 38. L. A. Ehrman, *et al.*, The LIM homeobox gene Isl1 is required for the correct
669 development of the striatonigral pathway in the mouse. *Proc. Natl. Acad. Sci. U.*
670 *S. A.* **110**, E4027 (2013).
671 39. Z. Xu, *et al.*, SP8 and SP9 coordinately promote D2-type medium spiny neuron
672 production by activating Six3 expression. *Development* **145** (2018).
673 40. K. M. Sousa, *et al.*, Wnt2 regulates progenitor proliferation in the developing
674 ventral midbrain. *J. Biol. Chem.* **285**, 7246–7253 (2010).
675 41. P. K. Multani, *et al.*, VMAT1 deletion causes neuronal loss in the hippocampus
676 and neurocognitive deficits in spatial discrimination. *Neuroscience* **232**, 32–44
677 (2013).
678 42. J. M. Revest, *et al.*, Adult hippocampal neurogenesis is involved in anxiety-
679 related behaviors. *Mol. Psychiatry* **14**, 959–967 (2009).

680 43. C. Anacker, R. Hen, Adult hippocampal neurogenesis and cognitive flexibility-
681 linking memory and mood. *Nat. Rev. Neurosci.* **18**, 335–346 (2017).
682 44. K. M. Tye, *et al.*, Amygdala circuitry mediating reversible and bidirectional
683 control of anxiety. *Nature* **471**, 358–362 (2011).
684 45. P. H. Janak, K. M. Tye, From circuits to behaviour in the amygdala. *Nature* **517**,
685 284–292 (2015).
686 46. M. P. de la Mora, A. Gallegos-Cari, Y. Arizmendi-García, D. Marcellino, K.
687 Fuxe, Role of dopamine receptor mechanisms in the amygdaloid modulation of
688 fear and anxiety: Structural and functional analysis. *Prog. Neurobiol.* **90**, 198–
689 216 (2010).
690 47. S. R. Hansson, B. J. Hoffman, É. Mezey, Ontogeny of vesicular monoamine
691 transporter mRNAs VMAT1 and VMAT2. I. The developing rat central nervous
692 system. *Dev. Brain Res.* **110**, 135–158 (1998).
693 48. E. A. Murray, The amygdala, reward and emotion. *Trends Cogn. Sci.* **11**, 489–
694 497 (2007).
695 49. J. Posner, *et al.*, Alterations in amygdala-prefrontal circuits in infants exposed to
696 prenatal maternal depression. *Transl. Psychiatry* **6**, e935 (2016).
697 50. X. Chang, *et al.*, RNA-seq analysis of amygdala tissue reveals characteristic
698 expression profiles in schizophrenia. *Transl. Psychiatry* **7**, e1203 (2017).
699 51. T. A. Avino, *et al.*, Neuron numbers increase in the human amygdala from birth
700 to adulthood, but not in autism. *Proc. Natl. Acad. Sci. U. S. A.* **115**, 3710–3715
701 (2018).

52. T. Asari, *et al.*, Amygdalar enlargement associated with unique perception. *Cortex* **46**, 94–99 (2010).

53. K. Rice, B. Viscomi, T. Riggins, E. Redcay, Amygdala volume linked to individual differences in mental state inference in early childhood and adulthood. *Dev. Cogn. Neurosci.* **8**, 153–163 (2014).

54. K. C. Bickart, C. I. Wright, R. J. Dautoff, B. C. Dickerson, L. F. Barrett, Amygdala volume and social network size in humans. *Nat. Neurosci.* **14**, 163–164 (2011).

55. J. Sallet, *et al.*, Social network size affects neural circuits in macaques. *Science* **334**, 697–700 (2011).

56. S. Atzil, *et al.*, Dopamine in the medial amygdala network mediates human bonding. *Proc. Natl. Acad. Sci. U. S. A.* **114**, 2361–2366 (2017).

57. K. C. Bickart, B. C. Dickerson, L. F. Barrett, The amygdala as a hub in brain networks that support social life. *Neuropsychologia* **63**, 235–248 (2014).

58. C. Schreiweis, *et al.*, Humanized Foxp2 accelerates learning by enhancing transitions from declarative to procedural performance. *Proc. Natl. Acad. Sci. U. S. A.* **111**, 14253–14258 (2014).

59. F. Zhu, R. R. Nair, E. M. C. Fisher, T. J. Cunningham, Humanising the mouse genome piece by piece. *Nat. Commun.* **10**, 1845 (2019).

60. N. R. Wray, *et al.*, Genome-wide association analyses identify 44 risk variants and refine the genetic architecture of major depression. *Nat. Genet.* **50**, 668–681 (2018).

724 61. S. Ripke, *et al.*, Biological insights from 108 schizophrenia-associated genetic
725 loci. *Nature* **511**, 421–427 (2014).
726 62. M. T. Lo, *et al.*, Genome-wide analyses for personality traits identify six
727 genomic loci and show correlations with psychiatric disorders. *Nat. Genet.* **49**,
728 152–156 (2017).
729 63. F. W. Lohoff, *et al.*, Association between polymorphisms in the vesicular
730 monoamine transporter 1 gene (VMAT1/SLC18A1) on chromosome 8p and
731 schizophrenia. *Neuropsychobiology* **57**, 55–60 (2008).
732 64. A. Waterhouse, *et al.*, SWISS-MODEL: homology modelling of protein
733 structures and complexes. *Nucleic Acids Res.* **46**, W296–W303 (2018).
734 65. Y. Choi, A. P. Chan, PROVEAN web server: a tool to predict the functional
735 effect of amino acid substitutions and indels. *Bioinformatics* **31**, 2745–2747
736 (2015).
737 66. P. Kumar, S. Henikoff, P. C. Ng, Predicting the effects of coding non-
738 synonymous variants on protein function using the SIFT algorithm. *Nat. Protoc.*
739 **4**, 1073–1081 (2009).
740 67. C. H. M. Rodrigues, D. E. V. Pires, D. B. Ascher, DynaMut: predicting the
741 impact of mutations on protein conformation, flexibility and stability. *Nucleic*
742 *Acids Res.* **46**, W350–W355 (2018).
743 68. M. Hashimoto, Y. Yamashita, T. Takemoto, Electroporation of Cas9
744 protein/sgRNA into early pronuclear zygotes generates non-mosaic mutants in
745 the mouse. *Dev. Biol.* **418**, 1–9 (2016).

746 69. J. P. Concordet, M. Haeussler, CRISPOR: Intuitive guide selection for
747 CRISPR/Cas9 genome editing experiments and screens. *Nucleic Acids Res.* **46**,
748 W242–W245 (2018).
749 70. R. B. Kline, *Principles and Practice of Structural Equation Modeling*, D. A.
750 Kenny, T. D. Little, Eds., 4th Edi. (The Guilford Press, 2016).
751 71. S. Chen, Y. Zhou, Y. Chen, J. Gu, fastp: an ultra-fast all-in-one FASTQ
752 preprocessor. *Bioinformatics* **34**, i884–i890 (2018).
753 72. A. Dobin, *et al.*, STAR: ultrafast universal RNA-seq aligner. *Bioinformatics* **29**,
754 15–21 (2013).
755 73. Y. Liao, G. K. Smyth, W. Shi, featureCounts: an efficient general purpose
756 program for assigning sequence reads to genomic features. *Bioinformatics* **30**,
757 923–930 (2014).
758 74. S. X. Ge, E. W. Son, R. Yao, iDEP: An integrated web application for
759 differential expression and pathway analysis of RNA-Seq data. *BMC*
760 *Bioinformatics* **19**, 1–24 (2018).
761 75. P. Langfelder, S. Horvath, WGCNA: An R package for weighted correlation
762 network analysis. *BMC Bioinformatics* **9**, 559 (2008).
763 76. P. Shannon, *et al.*, Cytoscape: a software environment for untegrated models.
764 *Genome Res.* **13**, 2498–2504 (2003).
765
766

767 **Tables and Figures**

768 **Table 1. *In silico* prediction of mVMAT1 tolerance to the humanized mutations**

769 **Asn133Thr and Asn133Ile.** Text in bold indicates significant effects of the

770 substitutions as predicted by Provean score < –2.5 or SIFT score < 0.05. The Provean

771 term "Deleterious" and SIFT term "Damaging" refer to significant effects on protein

772 function but do not necessarily indicate that they deteriorate protein function. All three

773 methods predict that 133Ile has greater effects than 133Thr on mVMAT1 function.

Ref.	Alt.	Provean		SIFT		DynaMut	
		Score	Prediction	Score	Prediction	ΔΔG (kcal/mol)	Prediction
Asn	Thr	**-3.27**	**Deleterious**	0.243	Tolerated	-0.062	Destabilizing
Asn	Ile	**-6.55**	**Deleterious**	**0.014**	**Damaging**	1.106	Stabilizing

774

775

776 **Table 2. List of gene ontology (GO) terms significantly overrepresented in the set**

777 **of differentially expressed genes (DEGs) between *Vmat1*^{WT} and *Vmat1*$^{Ile/Ile}$ mice.**

778 *P* values were corrected by the Benjamini-Hochberg method. Only terms with $P < 0.05$

779 are presented. Downregulation indicates *Vmat1*^{WT} > *Vmat1*$^{Ile/Ile}$ while upregulation

780 indicates *Vmat1*$^{Ile/Ile}$ > *Vmat1*^{WT}.

Direction	Pathways	Genes	adj.Pval
Upregulated	Regulation of cell junction assembly	*Ace*, *Cldn1*, *Enpp2*	5.5×10^{-3}
Downregulated	Locomotory behavior	*Gng7*, *Gpr88*, *Ido1*, *Pde1b*, *Penk*, *Ppp1r1b*, *Rasd2*	7.2×10^{-5}
Downregulated	Behavior	*Asic4*, *Foxp1*, *Gng7*, *Gpr88*, *Ido1*, *Pde1b*, *Penk*, *Ppp1r1b*, *Rasd2*	4.9×10^{-4}
Downregulated	Mononuclear cell differentiation	*Cd4*, *Foxp1*, *Pde1b*	2.8×10^{-3}
Downregulated	Response to amphetamine	*Pde1b*, *Ppp1r1b*, *Rgs9*	2.8×10^{-3}
Downregulated	Multicellular organismal response to stress	*Asic4*, *Gng7*, *Ido1*, *Penk*	2.8×10^{-3}
Downregulated	Cardiac muscle tissue development	*Foxp1*, *Myom3*, *Rarb*, *Rbp4*, *Wnt2*	3.9×10^{-3}
Downregulated	Regulation of cardiac muscle cell proliferation	*Foxp1*, *Rbp4*, *Wnt2*	4.0×10^{-3}
Downregulated	Behavioral fear response	*Asic4*, *Gng7*, *Penk*	4.6×10^{-3}
Downregulated	cAMP catabolic process	*Pde7b*, *Pde10a*	4.8×10^{-3}

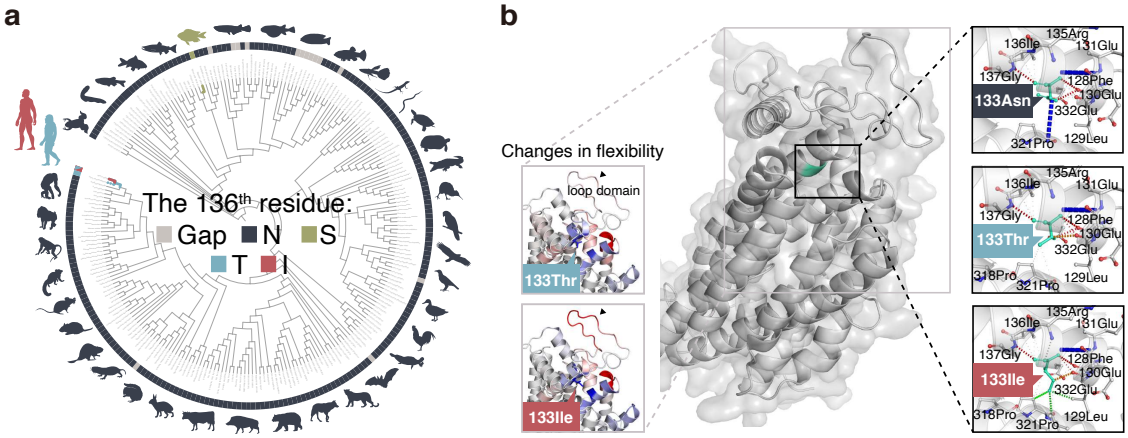

781

782 **Figure 1. An ultra-conserved residue in VMAT1 exhibits functional variants**

783 **unique to humans. (a)** A phylogenetic tree constructed by multiple sequence alignment

784 of the *VMAT1* gene. Almost all genes across 236 vertebrate species retain asparagine

785 (N, Asn) on the 136th residue, while humans are the only vertebrate species except for

786 bicolor damselfish (shown in green) with a unique polymorphism (T/I, Thr136Ile;

787 rs1390938). Note that the phylogenetic relationship presented here is not necessarily

788 consistent with the known species tree. **(b)** mVMAT1 protein structure predicted by

789 homology modeling and the effects of human-type mutagenesis (corresponding to

790 133Thr and 133Ile in mVMAT1). (Left) Δ Vibrational entropy energy between WT

791 (133Asn) and mutants. Amino acids are colored according to the vibrational entropy

792 change conferred by the given mutation. Red represents a gain of flexibility and blue

793 represents a rigidification of the structure. The 133Ile mutation leads to increased

794 flexibility of the first luminal loop, a receptor-like domain affecting the affinity of

795 ligands. (Right) When introduced *in silico*, 133Ile but not 13Thr exhibits hydrophobic

796 interactions (shown by green dotted line) with surrounding sites, which likely influence

797 the folding and/or stability of mVMAT1 protein. Blue, red, and orange dotted lines

represent amide bonds, hydrogen bonds, and weak van der Waals interactions, respectively.

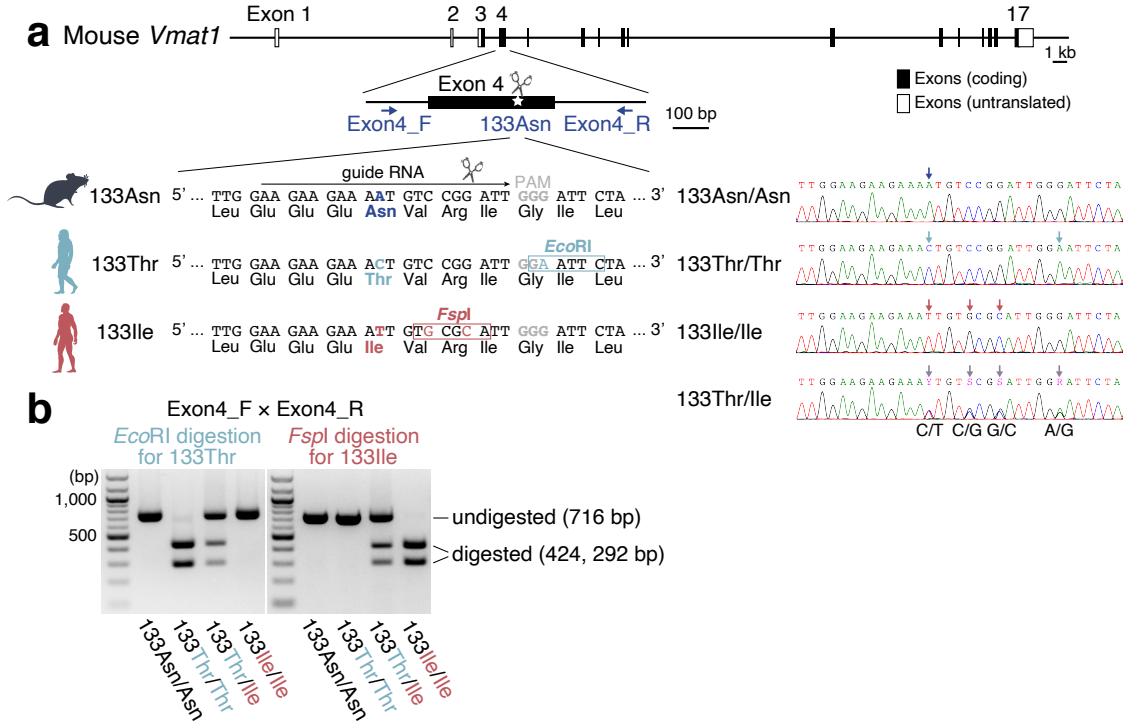

Figure 2. Generation of the *Vmat1*-humanized mouse models by CRISPR/Cas9 genome editing. (a) Targeting strategy for mVMAT1 133Asn humanization. Genetic configuration of the mouse *Vmat1* gene is shown above. Exon 4 encoding 133Asn is enlarged, and the primers used for genotyping (Exon4_F and Exon4_R) are depicted. To replace the mouse 133Asn with 133Thr or 133Ile by CRISPR/Cas9-mediated genome engineering, a guide RNA with minimum off-target effects was designed. GGG (gray) represents the PAM sequence. In addition to 133Asn humanization, restriction enzyme recognition sites (*Eco*RI and *Fsp*I) were synonymously incorporated to avoid the unwanted re-editing and to simplify genotyping. Sanger sequencing profiles of 133Asn/Asn (WT), 133Thr/Thr, 133Ile/Ile, and 133Thr/Ile are shown on the right. **(b)** PCR-RFLP assay, in which PCR products amplified using Exon4_F and Exon4_R were

813 digested by *Eco*RI and *Fsp*I, respectively, could be used to distinguish 4 genotypes

814 without sequencing.

815

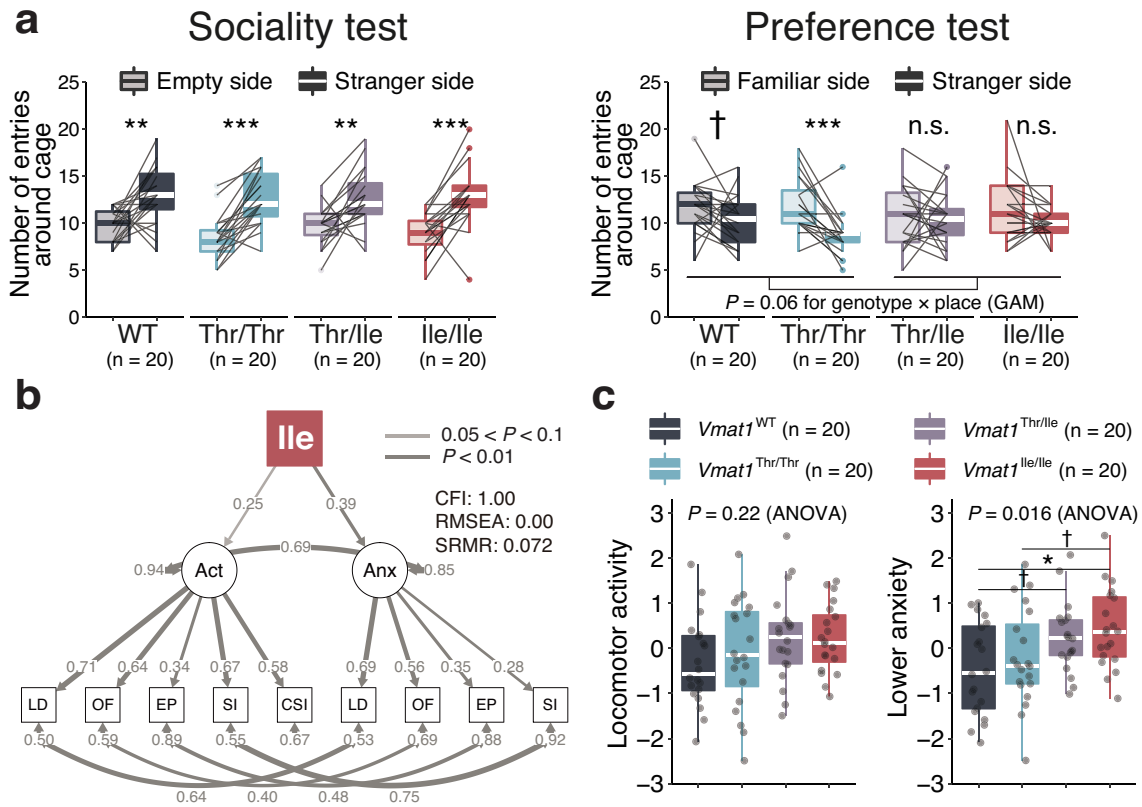

Figure 3. Comprehensive behavioral tests reveal distinct behavioral changes in *Vmat1*$^{Thr/Thr}$ and *Vmat1*^{Ile} mice, including reduced anxiety. (a) In Crawley's social interaction test, *Vmat1*$^{Thr/Thr}$ mice preferred a familiar (previously exposed) mouse over a novel stranger. **(b)** Structural Equation Modeling (SEM) revealed the best fit model to explain the effects of *Vmat1* genotype on locomotor activity (Act) and anxiety (Anx). According to the model, *Vmat1*^{Ile} (*Vmat1*$^{Thr/Ile}$ and *Vmat1*$^{Ile/Ile}$) significantly reduces anxiety-like behavior. The boxes and circles represent measured and latent variables, respectively. The paths represent causal relationships on which numerical values indicate standardized coefficient and the gray-scale intensity of the paths indicates statistical significance tested by *t*-test. See Methods for the detailed modeling procedure. **(c)** *Vmat1*^{Ile} mice exhibited lower anxiety than WT and *Vmat1*$^{Thr/Thr}$

genotypes. See Methods for the detailed calculation of the scores. For the composite anxiety score, a higher value indicates lower anxiety. Statistical significance was evaluated by paired *t*-test for **(a),** and by pair-wise *t*-test with FDR correction by the Benjamini-Hochberg method for **(c)**. Interactive effects of genotype (Ile allele labeled by 1, and 0 otherwise) and cage place were also assessed by generalized additive model with quasi-Poisson distribution in **(a)**. †: $0.05 < P < 0.1$, *: $0.01 < P < 0.05$, **: $0.001 < P < 0.01$, ***: $P < 0.001$.

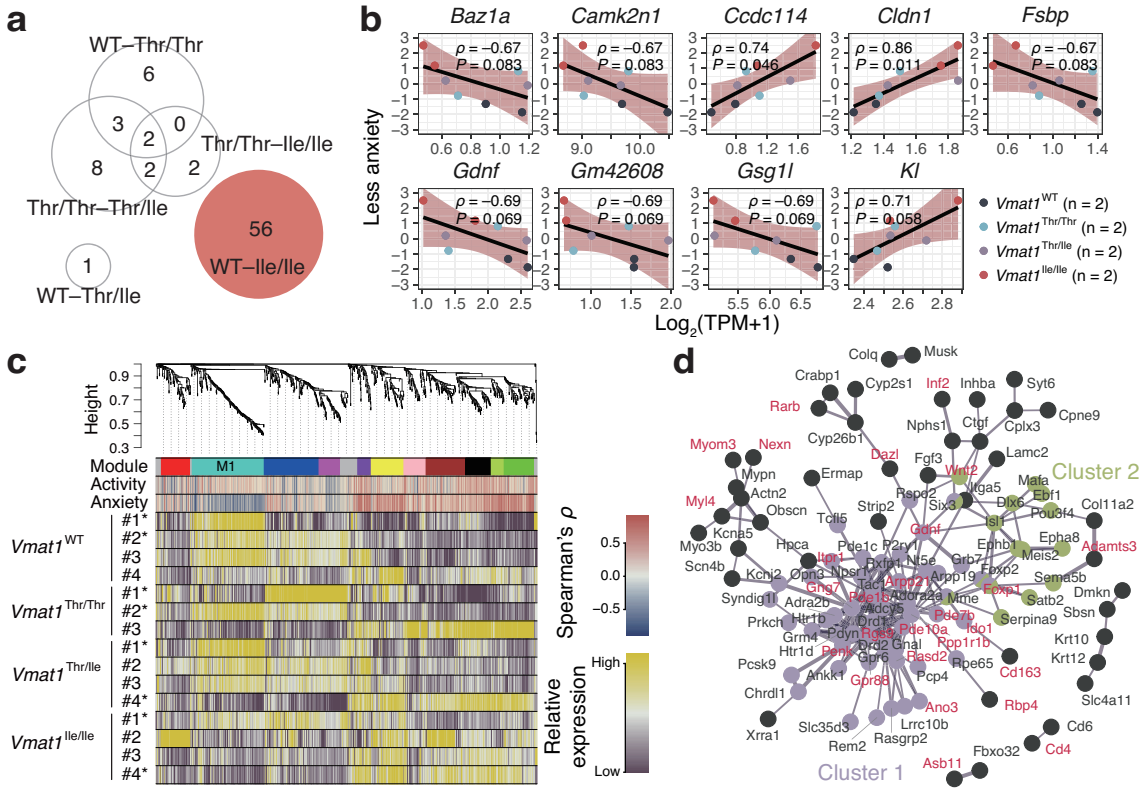

Figure 4. Differentially expressed genes (DEGs) in the brain among *Vmat1* genotypes and predicted co-expressing modules. **(a)** The number of DEGs detected by pair-wise comparisons among the four genotypes. All DEGs were found in the amygdala (with none in prefrontal cortex or striatum). **(b)** Correlations between individual DEG expression levels for the WT vs. and *Vmat1*$^{Ile/Ile}$ comparison and composite anxiety scores from LD, EP, OF, and SI tests (see Methods). Only genes with strong Spearman's correlations ($P < 0.1$) are shown. The bands are 95% confidence intervals. **(c)** Network dendrogram from co-expression modules based on the expression data of all 47 regional brain samples. Each branch represents an individual gene, and the colors below represent the module, correlation (ρ) with behavioral phenotype (locomotor activity and anxiety), and the relative expression level in the amygdala across genotypes. The samples with asterisks are from mice with behavioral data and

849 were used to calculate the correlations between expression levels and behavioral

850 phenotypes. The M1 module (shown in turquoise), showing negative correlations with

851 anxiety score exhibited significant overrepresentation of the DEGs detected between

852 WT and *Vmat1*$^{Ile/Ile}$ mice. **(d)** Protein–protein interaction networks among the genes in

853 M1. The DEGs detected between WT and *Vmat1*$^{Ile/Ile}$ mice are shown in red. The

854 thickness of the line indicates the strength of data support analyzed by STRING.

855

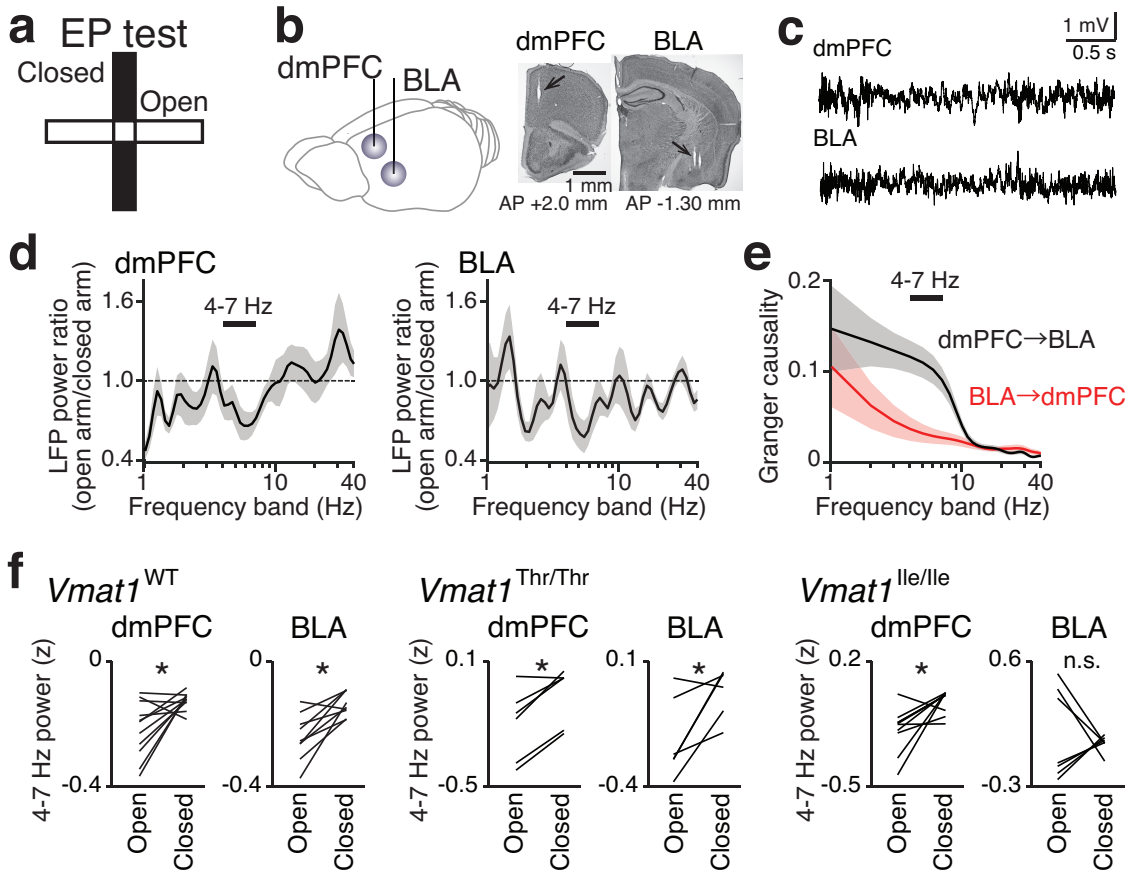

Figure 5. Wild-type and *Vmat1*$^{Thr/Thr}$ mice, but not *Vmat1*$^{Ile/Ile}$ mice, exhibit a reduction in amygdalar 4–7 Hz local field potential (LFP) power under anxiogenic conditions. (a) (Left) LFP recordings were simultaneously performed from the dorsomedial prefrontal cortex (dmPFC) and basolateral amygdala (BLA). (Right) Histological confirmation of electrode locations in the dmPFC and BLA. **(b)** Typical LFP signals from the dmPFC and BLA. **(c)** An elevated plus maze (EP) test. **(d)** Spectrograms of dmPFC (left) and BLA (right) LFP power in (anxiogenic) open arms relative to closed arms. Data were averaged from all *Vmat1*^{WT} mice. The bar above indicates the 4–7 Hz band, showing pronounced decreases in LFP power in both regions. **(e)** Spectral Granger causality averaged over 20 dmPFC–BLA electrode pairs.

867 **(f)** Comparison of dmPFC and BLA LFP 4–7 Hz power (z-scored) between open and

868 closed arms. *$P < 0.05$, paired *t*-test. Each line represents one electrode.

869

870